LANGMUIR

pubs.acs.org/Langmuir Article

Adsorption of Fatty Acid Molecules on Amine-Functionalized Silica Nanoparticles: Surface Organization and Foam Stability

Yingzhen Ma, Yao Wu, Jin Gyun Lee, Lilin He, Gernot Rother, Anne-Laure Fameau, William A. Shelton, and Bhuvnesh Bharti*

Cite This: *Langmuir* 2020, 36, 3703−3712 Read Online

ACCESS | Metrics & More | Article Recommendations | Supporting Information

ABSTRACT: The crucial roles of the ionization state and counterion presence on the phase behavior of fatty acid in aqueous solutions are well-established. However, the effects of counterions on the adsorption and morphological state of fatty acid on nanoparticle surfaces are largely unknown. This knowledge gap exists due to the high complexity of the interactions between nanoparticles, counterions, and fatty acid molecules in aqueous solution. In this study, we use adsorption isotherms, small angle neutron scattering, and all-atom molecular dynamic simulations to investigate the effect of addition of ethanolamine as a counterion on the adsorption and self-assembly of decanoic acid onto aminopropyl-modified silica nanoparticles. We show that the morphology of the fatty acid assemblies on silica nanoparticles changes from discrete surface patches to a continuous bilayer by increasing concentration of the counterion. This morphological behavior of fatty acid on the oppositely charged nanoparticle surface alters the interfacial activity of the fatty acid−nanoparticle complex and thus governs the stability of the foam formed by the mixture. Our study provides new insights into the structure−property relationship of fatty acid−nanoparticle complexes and outlines a framework to program the stability of foams formed by mixtures of nanoparticles and amphiphiles.

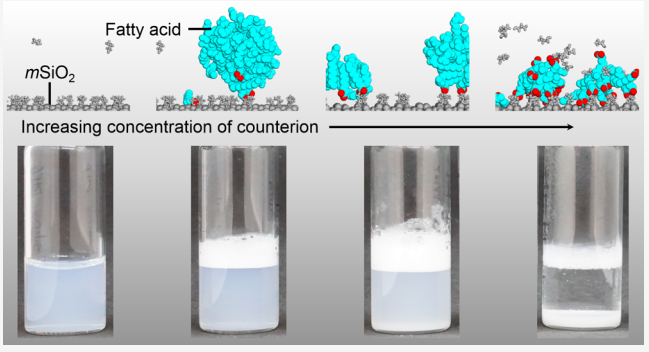

1. INTRODUCTION

The aggregative adsorption of amphiphilic molecules on colloids governs the optical properties, interfacial activity, and stability of the particles in the dispersion.[1−6] The self-assembled state of amphiphilic molecules on colloidal particles is dependent on the interaction between: (1) particle surface and unadsorbed amphiphilic molecules, (2) amphiphilic molecules adsorbed on the surface and unadsorbed molecules in bulk solution, and (3) among the molecules adsorbed on the surface.[7−9] These interactions determine the morphology of surface-adsorbed aggregates of amphiphilic molecules and govern the interfacial activity of the colloidal particles with adsorbed amphiphiles. The adsorption mechanism and morphology of the surface aggregates formed by synthetic amphiphiles, such as non-ionic surfactants, onto hydrophilic nanoparticles are well-known and characterized.[10−12] However, the equilibrium morphology of natural amphiphiles, such as fatty acids, adsorbed onto nanoparticles in the presence of organic counterions and their impact on the interfacial activity of nanoparticles are poorly understood. This lack in understanding is due to the complexity of the phase behavior of fatty acid molecules on the nanoparticles, which is highly dependent on the concentration of counterions in the dispersion medium.[13,14]

Fatty acids are a class of naturally occurring amphiphiles consisting of an aliphatic hydrocarbon chain and carboxylic acid polar head group.[15] The carboxylic acid head group can exist in either the protonated (−COOH) or deprotonated ($-COO^-$) state, which is primarily governed by the presence of counterion molecules in solution.[16] The concentration of the counterion in the solution also governs the morphology of the self-assembled state of the fatty acid molecules and their Kraft temperature. Previously, it has been shown that increasing the fatty acid-to-counterion molar ratio in aqueous solution drives morphological transitions in the self-assembled state of the fatty acids from disc-like micelles, to multilamellar tubules, to discrete spherical micelles.[17,18] Despite the rich phase behavior of the fatty acid molecules in bulk, the effects of the ionization state of fatty acids on their adsorption onto hydrophilic nanoparticles remain unknown. The self-assembled state and phase behavior of fatty acid in aqueous solution

Received: January 18, 2020
Revised: March 20, 2020
Published: March 22, 2020

https://dx.doi.org/10.1021/acs.langmuir.0c00156
Langmuir 2020, 36, 3703−3712

containing nanoparticles are impacted by the chemical design of the fatty acid molecules, size of the nanoparticles, and environmental parameters such as temperature, salinity, and the presence of counterions.[19−21] Understanding the interactions governing the self-assembly and phase behavior of fatty acids adsorbed at nanoparticles is critical to the development of multifunctional materials with tunable interfacial and bulk properties, such as foam stability and viscoelasticity.[22] In this study, we systematically probe the effect of increasing counterion concentration on the adsorption and self-assembled state of fatty acid molecules on the surface of hydrophilic nanoparticles, and investigate its corresponding impact on the interfacial activity of the fatty acid−nanoparticle complex.

We use adsorption isotherm, small angle neutron scattering (SANS), and all-atom molecular dynamic (MD) simulations to understand the effect of an increasing concentration of counterions on the adsorbed amount, and the morphology of the fatty acid molecules formed at amine functionalized hydrophilic nanoparticles. We use decanoic acid ($C_9H_{19}COOH$) and ethanolamine ($HOCH_2CH_2NH_2$) as model fatty acid molecules and counterions, respectively, and propyl amine ($-C_3H_6NH_2$)-functionalized spherical silica (mSiO$_2$) as model hydrophilic nanoparticles. We find that the counterion-to-fatty acid molar ratio not only determines the amount of fatty acid adsorbed on the silica nanoparticles but also governs the morphology of the fatty acid assemblies formed at the mSiO$_2$ surface. Furthermore, we demonstrate that the morphological change of fatty acid at mSiO$_2$ impacts the interfacial activity of the composite structure, thus altering the stability of foam formed by the dispersion. This study outlines the relationship of the counterion-tuned structure of fatty acid assemblies on silica nanoparticles to the interfacial activity of the composite structure, and provides insights into the principle of designing nanomaterials with tunable foaming properties.

2. RESULTS AND DISCUSSION

2.1. Nanoparticle Synthesis and Characterization.

2.1.1. Amine Functionalization of Silica Nanoparticles. The propylamine-functionalized silica nanoparticles were synthesized by controlled surface modification of commercially available Ludox-TMA colloidal silica (Sigma-Aldrich). The silica nanoparticle dispersion was dialyzed for 7 days using ultrapure water with a resistivity of 18.2 MΩ-cm, changing water every day to remove any undesired foreign molecules in the dispersion. In a typical synthesis, 22.2 g of 27 wt % Ludox-TMA dispersion was mixed with 12 mL of acetic acid and 3.8 mL of deionized water (Figure 1a and Figure S1). The mixture was transferred into a round-bottom flask, fitted with a reflux condenser, and heated to 80 °C. After 30 min of equilibration, 0.7 mL of (3-aminopropyl)triethoxysilane (APTES) was added to the flask containing the mixture with constant stirring. The mixture was reacted for 16 h at 80 °C under reflux. The dispersion containing modified silica nanoparticles was removed from the flask and dialyzed for 24 h using deionized water at pH 4. The larger aggregates from the dialyzed mSiO$_2$ were removed by filtering it through a syringe filter with a pore size of 220 nm. The pH of the filtered nanoparticle solution was adjusted to 4, and the mSiO$_2$ dispersion was stored at 4 °C.

2.1.2. Characterization of mSiO$_2$. The mSiO$_2$ nanoparticles were characterized for their size and surface charge by small angle X-ray scattering (SAXS), a scanning electron microscope

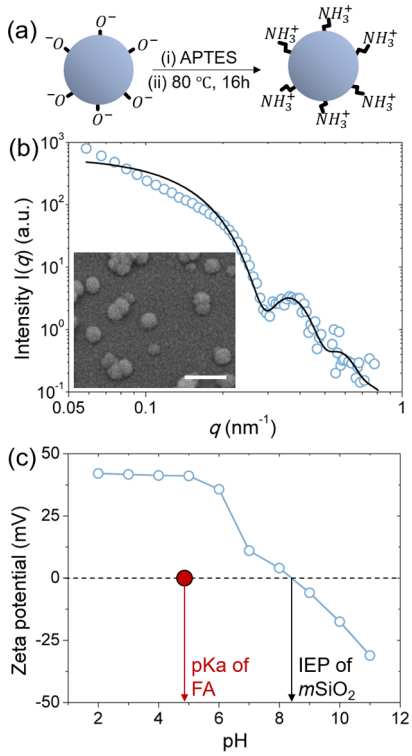

Figure 1. (a) Schematic representation of the synthesis of aminopropyl functionalized silica nanoparticles (mSiO$_2$). The aminopropyl groups ($-C_3H_6NH_2$) were chemically grafted onto commercially available Ludox-TMA silica nanoparticles and then protonated to $-C_3H_6NH_3^+$. (b) Experimental SAXS profiles (blue circles) for mSiO$_2$ nanoparticles in deionized water at pH 7. Solid line represents the fit to the experimental data using the form factor of polydisperse spheres. Inset: SEM image showing spherical shape of mSiO$_2$ nanoparticles. The scale bar in the inset is 100 nm. (c) Zeta potential−pH titration curve for the mSiO$_2$ nanoparticles in deionized water. The red line at pH 4.9 represents the pK_a of the carboxylic acid group of decanoic acid in water. The black line indicates the isoelectric point of mSiO$_2$ nanoparticles.

(SEM), and zeta potential-pH titration. The bulk size characterization of mSiO$_2$ was performed using SAXS (Xenocs Xeuss 2.0). The SAXS profiles for 0.1% by weight of mSiO$_2$ at pH 7 is shown in Figure 1b where $I(q)$ is the scattering intensity, and q is the scattering momentum transfer related to the X-ray wavelength (λ) and scattering angle (θ) as $q = \left(\frac{4\pi}{\lambda}\right)\sin\left(\frac{\theta}{2}\right)$. The experimentally measured scattering profile is fitted using a spherical form factor model with log-normal particle size distribution (Figure 1b). The form factor model is effective in representing the scattering at $q > 0.2$ nm^{-1} but fails in the region $q < 0.2$ nm^{-1}. This disagreement between the experimental data and form factor model is caused by weak aggregation of the nanoparticles at pH 7 (zeta potential < +15 mV, Figure 1c), which results in an increase in scattering intensity at $q < 0.2$ nm^{-1}. Despite the presence of the structure factor, the form factor provides the accurate nanoparticle diameter of 30 nm, with a polydispersity index of 0.1, which agrees with SEM imaging (Figure 1b, inset). The surface charge on mSiO$_2$ is quantified using zeta potential measurement (Litesizer 500, Anton Paar GmbH) as a function of pH (Figure 1c). The experimental results show that the zeta potential of mSiO$_2$ changes from +42.7 to −31.1 mV as pH is increased from 2 to 11, and the isoelectric point of mSiO$_2$

https://dx.doi.org/10.1021/acs.langmuir.0c00156
Langmuir 2020, 36, 3703−3712

nanoparticles is pH ∼8.5. The isoelectric point of the native silica nanoparticles is pH ∼2,[23] but it changes to pH ∼8.5 upon surface modification with propylamine surface groups (Figure S1). The change in the isoelectric point of silica nanoparticles upon surface chemical modification is attributed to the protonation of the aminopropyl functional group[24] at pH <8. The positive charge on the surface of mSiO$_2$ at pH < 8 is key in directing the adsorption and corresponding self-assembled state of the fatty acid molecules on the surface of mSiO$_2$ nanoparticles.

2.2. Adsorption of Fatty Acid on mSiO$_2$. In this study, we use decanoic acid as model fatty acid and control its protonation state using ethanolamine as a counterion. We define the counterion-to-fatty acid molar ratio (R) as the ratio of the total number of ethanolamine to the fatty acid molecules in the solution. The value of R is equivalent to the fraction of the fatty acid molecules in the deprotonated state, i.e., $R \equiv \frac{n_{COO^-}}{n_{total}}$ where n_{COO^-} is the number of deprotonated fatty acid molecules, and n_{total} is the total number of fatty acid molecules in the solution. To understand the effect of the ionization state of fatty acid on its interaction with mSiO$_2$, we experimentally measure the adsorption isotherms of the decanoic acid onto mSiO$_2$ nanoparticles with R increasing from 0.05 to 1.0. The adsorption isotherms were measured at pH 6, where the net charge on mSiO$_2$ is positive and an electrostatic attraction exists between the deprotonated carboxylate group of the fatty acid and protonated propyl ammonium group on the surface of mSiO$_2$ nanoparticles.

The adsorption isotherms were measured using a well-established solvent depletion method.[25] In a typical adsorption experiment, increasing amounts of fatty acid at fixed R were added to 1 wt % mSiO$_2$ aqueous dispersion. The pH was adjusted to 6 by adding small amounts of 5 N aqueous HCl or NaOH solution. The mixture was equilibrated at 20 °C for 24 h, and then mSiO$_2$ with adsorbed fatty acid molecules was removed by centrifuging the dispersions at 18,000 RCF for 2 h. Electrostatic attraction between the oppositely charged fatty acid molecules and silica surfaces further drives fatty acid-mediated aggregation of mSiO$_2$ nanoparticles, thus destabilizing the dispersion. The aspect of aggregation of mSiO$_2$ nanoparticles into fractal superstructures, while interesting, is beyond the scope of this study focused on understanding the self-assembly of fatty acid molecules on nanoparticles.

Based on visual inspection of the sample and known adsorption mechanism of amphiphiles,[26] fatty acid molecules in their mixture with counterions and mSiO$_2$ are present in three distinct forms, namely, (a) undissolved fatty acid gel (c_u, protonated form, −COOH), (b) unadsorbed fatty acid in bulk solution (c_o, deprotonated form, −COO$^-$), and (c) adsorbed fatty acid onto mSiO$_2$ (c_{ads}, deprotonated form, −COO$^-$) as shown in Figure 2a. The fractions of total fatty acid concentration (c_t) existing in these three forms were determined by systematically separating the mixture using centrifugation. The mass density of the native protonated fatty acid is ∼ 0.893 g/cm^3;[27] therefore, the concentration of fatty acid in the undissolved gel form (c_u) was determined by physically collecting the pellets floating on the liquid−air interface in the vial after centrifugation. The pellets were dried overnight at room temperature to ensure complete evaporation of water. The concentration of undissolved fatty acid decreases with increasing R, as shown in Figure S2. The concentration of fatty acid dissolved in aqueous solution but unadsorbed onto

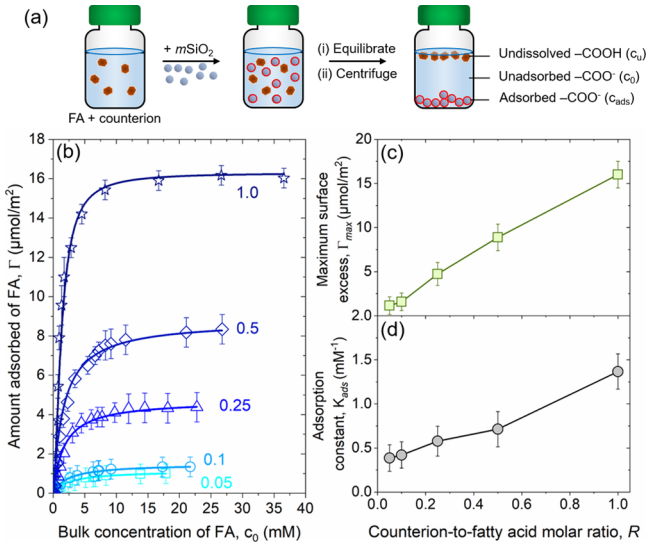

Figure 2. (a) Schematic of the solvent depletion method used for experimentally measuring the adsorption isotherm of fatty acid molecules onto mSiO$_2$ nanoparticles. Here, the acronym FA refers to fatty acid. (b) Adsorption isotherm for fatty acid on mSiO$_2$ at increasing counterion-to-fatty acid molar ratio (R). The discrete points are experimental values, and solid lines are fits using Langmuir adsorption model given by eq 1. (c) Maximum surface excess Γ_{max} and (d) adsorption constant K_{ads} of fatty acid on mSiO$_2$ with increasing R, as obtained by fitting the experimental data using Langmuir model.

mSiO$_2$ was determined by first carefully removing the aqueous supernatant from the centrifuged sample and then measuring the concentration of the fatty acid in the supernatant using surface tension. The surface tension of the supernatant was measured using an optical tensiometer (Attension Theta, Biolin Scientific) where the shape of the pendant droplet is analyzed using Young−Laplace equation.[26,28,29] The relationship between surface tension and concentration of the fatty acid in the supernatant was determined for different solutions with known concentrations, yielding a calibration curve, as shown in Figure S3. When the unknown concentration of deprotonated fatty acid in the supernatant was higher than critical micellization concentration (CMC) of the molecules, the unknown concentration was determined by systematic dilutions until the measured surface tension is below its characteristic value at CMC. The net unknown concentration of the supernatant was calculated by multiplying the concentration estimated for the diluted sample (from surface tension calibration curve) and the dilution factor. It should be noted that fatty acid molecules only in the deprotonated state (−COO$^-$) are surface-active and reduce the surface tension, as shown in Figures S3 and S4. Therefore, the surface tension measurements enable selective determination of concentration of fatty acid molecules in the dissolved (deprotonated) state.

The amount of fatty acid molecules adsorbed onto mSiO$_2$ nanoparticles (Γ) is obtained from the equation $\Gamma = c_{ads}V/m_s$ where V is the volume of the aqueous solution, m_s is the mass of mSiO$_2$ in bulk solution, $c_{ads} = c_t - (c_o + c_u)$ is the concentration of fatty acid molecules adsorbed onto mSiO$_2$, c_t is the total concentration of fatty acid, c_o is the concentration of dissolved but unadsorbed fatty acid in the solution, and c_u is the concentration of undissolved fatty acid molecules (Figure 2a). It should be noted that for R = 1, the value of c_u = 0, i.e.,

https://dx.doi.org/10.1021/acs.langmuir.0c00156
Langmuir 2020, 36, 3703−3712

all fatty acid exists in dissolved states, i.e., unadsorbed and adsorbed states on nanoparticles (deprotonated form, $-COO^-$) and for $R = 0$, $c_u = c_t$, i.e., the fatty acid molecules exist only as an undissolved gel state (protonated form, $-COOH$). The adsorption isotherms of fatty acid molecules bound to mSiO$_2$ nanoparticles at five R values are shown in Figure 2b. At all tested counterion concentrations, the amount of fatty acid adsorbed on mSiO$_2$ shows an initial increase followed by a plateau, which is a characteristic of the molecular adsorption on a surface with a fixed number of binding sites.[26] These experimentally measured adsorption isotherms can be represented by a Langmuir adsorption model given as[30]

$$\Gamma = \frac{\Gamma_{max} K_{ads} c_o}{1 + K_{ads} c_o} \quad (1)$$

Here, Γ is the amount of fatty acid adsorbed onto mSiO$_2$, Γ_{max} is the maximum surface excess of fatty acid, c_o is the equilibrium concentration of dissolved but unadsorbed fatty acid in bulk, K_{ads} is the equilibrium adsorption constant, which is proportional to the binding affinity of the fatty acid molecules to mSiO$_2$ nanoparticles. The Langmuir model is the simplest two-parameter model that allows representing the maximum amount of fatty acid adsorbed and its binding affinity for mSiO$_2$ in terms of Γ_{max} and K_{ads}.

The experimental adsorption isotherm data are fitted using the Langmuir model given in eq 1 (Figure 2b) keeping Γ_{max} and K_{ads} as free fit parameters. The values of Γ_{max} and K_{ads} as obtained by the least square fitting of experimental data with increasing R are shown in Figure 2c,d. We find that Γ_{max} increases (nearly) linearly with increasing R. The values of Γ_{max} increased from 1.0 to 16.0 μmol/m^2 (Figure 2c) as R increased from 0.05 to 1.0, i.e., the number of fatty acid molecules adsorbed onto mSiO$_2$ increases with increasing R. The observed linear increase in the maximum surface excess of fatty acid molecules can be attributed to the linear increase in the concentration of deprotonated (negatively charged carboxylate) fatty acid molecules with increasing R.[13]

We find that K_{ads} shows only a slight increase from 0.4 to 1.4 mM^{-1} with R increasing from 0.05 to 1.0. This slight increase in K_{ads} with R is an indicative of the small increase in adsorption free energy of the fatty acid molecules at the mSiO$_2$ surface. It should be noted that because pH of the aqueous solution was kept fixed (at pH 6), the surface charge of mSiO$_2$ can be approximated as constant for all R. Assuming that the charging of the silica and fatty acid molecules involves monovalent ions only and that the surface change density of mSiO$_2$ at pH 6 is low, the free energy of adsorption can be calculated from K_{ads} as $\Delta G^o_{ads} = -N_A k_B T \ln(55.5 \times K_{ads})$ where N_A is the Avogadro number, k_B is the Boltzmann constant, and T is the temperature.[31,32] We find that the magnitude of ΔG^o_{ads} increases from -24.2 to -27.4 kJ/mol upon increasing R from 0.05 to 1. Two key conclusions drawn from these values are: first, the value of ΔG^o_{ads} is lower than the adsorption free energy of cationic surfactants on the silica surface. This lowering of adsorption free energy in our case can be attributed to the smaller surface charge density on the synthesized mSiO$_2$ nanoparticles.[33] Second, only a small increase in ΔG^o_{ads} highlights that the chemical nature of the functional group binding to mSiO$_2$ at low and high R values is similar, which is the carboxylate group of the decanoic acid. The adsorption isotherms show that the amount of fatty acid bound onto mSiO$_2$ increases but do not provide any insights into the self-assembled state and morphology of the surface-adsorbed molecules. To uncover the self-assembled state of the fatty acid on mSiO$_2$ nanoparticles, we perform small angle neutron scattering analysis for dispersions of mSiO$_2$ with adsorbed fatty acid, as discussed in the next section.

2.3. Morphology of Fatty Acid Adsorbed onto mSiO$_2$.

2.3.1. Small Angle Neutron Scattering Experiments. An increase in the counterion-to-fatty acid molar ratio leads to an increase in the amount of fatty acid molecules adsorbed on mSiO$_2$ nanoparticles. This increase in surface adsorption of fatty acid molecules drives a morphological change in the fatty acid assemblies formed on the surface of mSiO$_2$ nanoparticles. Here, we characterize the morphology of the fatty acid molecules on mSiO$_2$ using SANS. The experiments were carried out at silica contrast-matched condition where 62.5 wt % deuterium oxide (D_2O) and 37.5 wt % H_2O were used as the solvent.[10,12] Therefore, the neutron scattering originated solely from the fatty acid molecules and their assemblies in the solution. The SANS experiments were performed at ORNL HFIR facility using the GP-SANS instrument with pinhole collimation at a neutron wavelength of 6 Å. Further details about the SANS experiments can be found in previous publications.[34,35]

The SANS experiments were performed at constant total concentrations of fatty acid and mSiO$_2$, with increasing counterion-to-fatty acid molar ratio from $R = 0.05$ to 1.0. The maximum concentration of fatty acid molecules adsorbed onto silica at $R = 1.0$ is given by

$$C_{max} = \frac{\Gamma_{max} \times A_{mSiO_2} \times W_{mSiO_2}}{V_{total} \times 10^{-3}} \quad (2)$$

where C_{max} is the total concentration of fatty acid at Γ_{max}, A_{mSiO_2} and W_{mSiO_2} are the specific surface area and weight of mSiO$_2$ nanoparticles in the solution, respectively, and V_{total} is the total volume of the sample. Here, the fatty acid concentration was 0.03 M, which was equivalent to the 0.5 C_{max} at $R = 1.0$ (Figure 2b). Therefore, for SANS at $R < 1.0$ the fatty acid existed in three states as discussed in the previous section (Figure 2a). The undissolved fatty acid floats on the surface of the solution; therefore, the incoming neutron beam selectively probes the protonated fatty acid in the aqueous solution (both adsorbed and unadsorbed). The SANS profiles for mSiO$_2$ with adsorbed fatty acid under silica contrast-matched conditions with increasing R, at pH 6 and 20 °C, are shown in Figure 3a. The mSiO$_2$ nanoparticles in the presence of fatty acid exist as aggregates and tend to phase separate. During our SANS measurements, these aggregates settle and only a small unknown fraction of the particles with adsorbed fatty acid remain in the neutron beam. Because of the lack of information of the exact amount of the silica–fatty acid composite in the neutron beam, the scattering intensity is represented in arbitrary units. The curves show an increase in the low-q (< 0.15 nm^{-1}) scattering with $I(q) \propto q^{-2}$. This proportional increase in the scattering intensity is likely a combination of the scattering due to the fatty acid-mediated aggregation of mSiO$_2$ nanoparticles, and the presence of fatty acid gel phase clusters in the solution. The SANS profiles also show enhancement of the primary form factor oscillation at $q \sim 0.15$ nm^{-1} with increasing R. Additionally, the primary minima show a slight shift to higher q values upon increasing R (Figure 3b), indicating a decrease in the size of fatty acid assemblies on mSiO$_2$ nanoparticles. Detailed characteristics of

https://dx.doi.org/10.1021/acs.langmuir.0c00156
Langmuir 2020, 36, 3703−3712

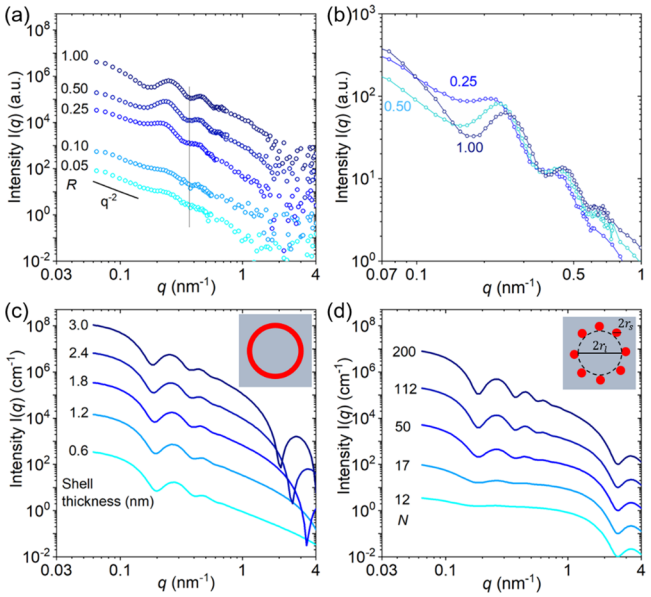

Figure 3. (a) SANS profiles for fatty acid molecules adsorbed on mSiO$_2$ nanoparticles in H_2O/D_2O mixture matching the scattering length density of silica. The profiles were measured at increasing R from 0.05 to 1.0. The curves are shifted by a constant factor of 10 for better visualization. (b) Zoomed-in plot of the scattering intensity from q = 0.07 to 1 nm^{-1}. The primary minima of SANS profile shifts to higher q values upon increasing R, indicating a decrease in the characteristic size of the self-assemblies formed by fatty acid molecules on mSiO$_2$ upon increasing counterion concentration. (c, d) Simulated SANS profiles using spherical shell and raspberry-like form factor models, respectively. The spherical shell form factor model provides poor representation of the experimental data (shown in (a)) both qualitatively and quantitatively. The primary oscillation of raspberry-like form factor model qualitatively represents the experimental SANS data and captures the change in the morphology of adsorbed fatty acid. The inserts in (c) and (d) are the respective conceptual schematics of the used form factor models.

self-assemblies formed by molecules on nanoparticles can be obtained by fitting the experimental SANS data to theoretical form factor models. In our case, such model dependent analysis is not feasible because of too many unknown and unconstrained fit parameters. Therefore, we first perform model independent analysis of the SANS data using Porod's law and determine the change in the surface-to-volume ratio of the fatty acid assemblies with increasing R. According to Porod's law, the scattering intensity at large q ($\rightarrow \infty$) is represented as[36] $I(q) = \frac{2\pi(\Delta\rho^2)}{q^4}\frac{S}{V}$ where $\Delta\rho$ is the scattering length density contrast between the scattering object and surrounding medium, and $\frac{S}{V}$ is the surface area-to-volume ratio of the scattering object. Analyses of our SANS data (Figure S5) show approximately 10 times increase in the $\frac{S}{V}$ upon increasing R from 0.05 to 1.0. This increase in surface-to-volume ratio indicates a significant decrease in the size of self-assembled structures formed by fatty acid, highlighting a phase transition of fatty acid from the bulk gel phase to surface-adsorbed layer upon increasing counterion concentration. Note that since scattering intensity is in arbitrary units, the observed increase in the values of $\frac{S}{V}$ with increasing R only represents qualitative changes. A complete model-dependent SANS data analysis is limited due to the fatty acid-induced aggregation of mSiO$_2$ nanoparticles and corresponding emergence of the structure factor in the scattering profile, which requires additional parameters. Therefore, instead of direct fitting the experimental data, we systematically simulate the SANS profiles, which provide a qualitative information on the morphology of the assemblies formed by fatty acid molecules on mSiO$_2$ nanoparticles.

Previous studies have shown that amphiphilic molecules can adsorb onto nanoparticles in two morphological states, namely, continuous layers or discrete patches.[10] To investigate which of the two morphologies is formed by fatty acid molecules on mSiO$_2$, we test the applicability of the spherical shell and raspberry-like form factor models in representing the experimental SANS profiles. The spherical shell model represents the formation of a continuous layer of fatty acid on mSiO$_2$ nanoparticles.[2] Here, we simulate the SANS profiles using a shell model with a fixed core radius of 15 nm with a 0.1 polydispersity index (Figure 1b) and increasing the shell thickness from 0.6 to 3.0 nm (Figure 3c). These thickness values are used because of the characteristic length of the decanoic acid molecule, which is 1.2 nm;[37] therefore, 1.2 nm and 2.4 nm correspond to continuous homogeneous monolayer and bilayer structures, respectively. We find that the primary oscillation at $q \sim 0.25$ nm^{-1}, a characteristic of the shell structure, is present in all simulated cases, which is in qualitative disagreement with the experimental SANS profiles (Figure 3a,b) for $R < 0.5$. The experiments show the presence of a smeared oscillation at $R < 0.5$. This qualitative mismatch between the experimental and simulated SANS profiles suggests that the self-assembled state of the fatty acid on mSiO$_2$ is more complex than a continuous shell of fatty acid molecules formed on nanoparticles.

The second possible morphological state of fatty acid on mSiO$_2$ nanoparticles is discrete patches. Here, we test the presence of such configuration of fatty acid on the nanoparticles by simulating the scattering profile using a raspberry-like form factor. The model represents the form factor of a large sphere with small spheres randomly adsorbed on its surface.[38] The total scattering intensity of such a raspberry-like structure with a core particle contrast-matched with the continuous medium is given as[38−40]

$$I_{RB}(q) = \frac{N\phi_l V_s^2 \Delta\rho^2 \Psi_s^2}{16 V_l}\left[1 + (N-1)\left[\frac{\sin(q(r_l + r_s))}{q(r_l + r_s)}\right]^2\right] \quad (3)$$

$$\Psi_s = \frac{3[\sin(qr_s) - qr_s\cos(r_s)]}{(qr_s)^2} \quad (4)$$

where N is the number of small spheres of radius r_s, volume V_s and scattering contrast $\Delta\rho$ adsorbed onto the core particle, ϕ_l is the volume fraction of the core particle of radius r_l, volume V_l, and q is the scattering vector (see the Supporting Information for detailed derivation). The raspberry-like form factor model accounts for all the self-correlation and cross-correlation for small spheres randomly adsorbed onto a larger sphere.[38] The simulated SANS profiles for a contrast-matched sphere with an increasing number of surface-adsorbed smaller spheres are shown in Figure 3d. The profiles are simulated for core particle radius r_l = 15 nm, r_s = 4 nm with increasing N from 12 to 200. The simulated curves using raspberry-like form factor show an oscillation in the range 0.15 < q < 0.3 nm^{-1}. This oscillation is the signature of the characteristic correlation

https://dx.doi.org/10.1021/acs.langmuir.0c00156
Langmuir 2020, 36, 3703−3712

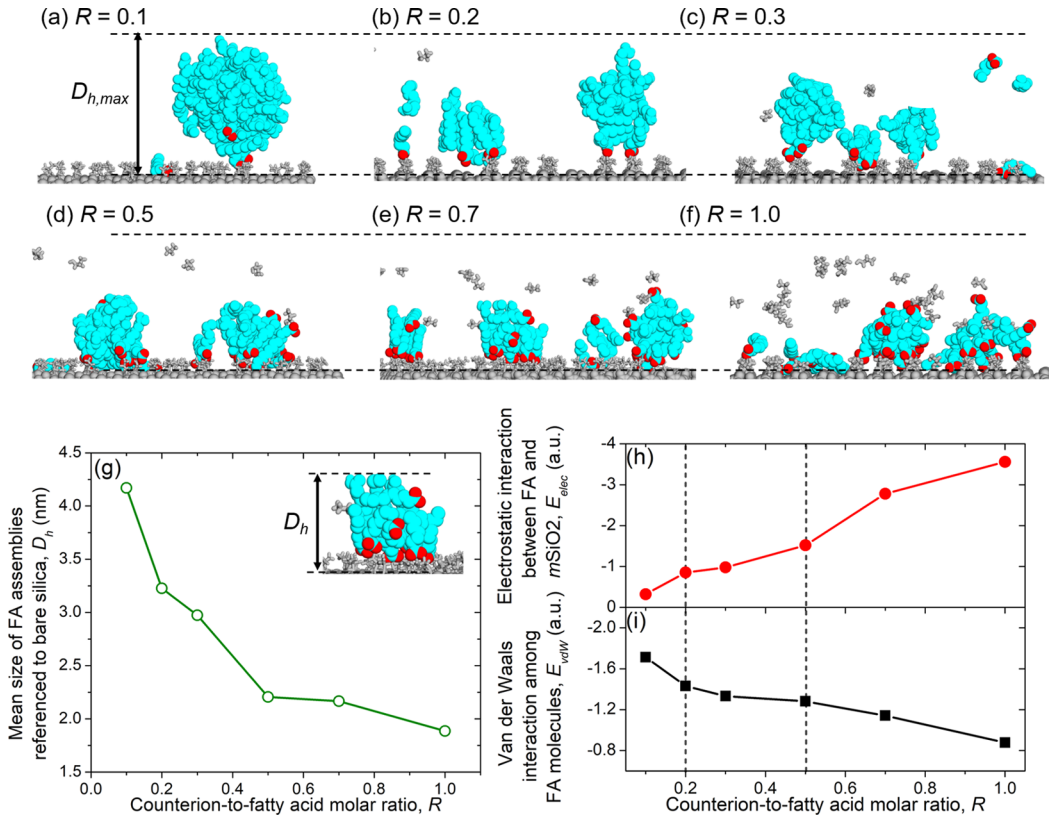

Figure 4. (a)−(f) Snapshots of equilibrated adsorbed state of fatty acid molecules on $m\mathrm{SiO_2}$ surface at different counterion-to-fatty acid molar ratios, R, increasing from 0.1 to 1.0. The dashed line is a reference line showing the height of the largest assembly at R = 0.1, $D_{h,\,max}$. Functional groups (propyl ammonium ions) and counterion molecules (ethanolamine) are drawn as grey licorice bonds. Bare silica is shown in grey solid van der Waals spheres. For fatty acid molecules, hydrogen atoms are hidden. All atoms in fatty acid molecules are colored in cyan, except the oxygen in the carboxylate ion is colored in red. Water and chloride molecules are not shown here for clarity. At R = 0.1, a large cluster of fatty acid with discrete negative charges is adsorbed on positively charged $m\mathrm{SiO_2}$ surface. As R is increased, the large assembly decomposes and tends to spread on $m\mathrm{SiO_2}$ surface, inducing a decrease in the size of surface aggregates, D_h. (g) Mean size of fatty acid assemblies formed on $m\mathrm{SiO_2}$ surface, D_h as a function of R, and the inset is the schematic representation of D_h. (h) Electrostatic interaction, E_{elec} between fatty acid assembly and $m\mathrm{SiO_2}$ surface and (i) van der Waals interaction between fatty acid molecules at different R values. In the Figure, FA refers to fatty acid.

distance between the surface adsorbed small spheres. The oscillation gets pronounced upon increasing N because of the increasing correlation in spatial distribution of the surface-adsorbed particles (fatty acid in our case), which is the characteristic diameter of the core particle (Figure 3d). The observed behavior of smearing of the primary oscillation at low N is characteristic of the nature of the surface adsorbed structures. At large N, the surface assembly of fatty acid resembles the continuous layer, and the spherical shell and raspberry-like form factor models yield similar results (Figure 3b,c). We acknowledge that the raspberry-like form factor is strictly applicable only in the case of spherical particles adsorbed onto a larger sphere, the model qualitatively captures the effect of the discrete nature of the surface-adsorbed assemblies on the scattering profile, especially at low surface loadings. In our experiments of fatty acid adsorbed on $m\mathrm{SiO_2}$, we observe similar smearing of the primary form factor oscillation at $R < 0.25$, highlighting the discrete nature of the fatty acid assemblies formed on $m\mathrm{SiO_2}$ nanoparticles. Upon increasing the counterion concentration to R above 0.50, the oscillation becomes pronounced, which agrees with the continuous layer of fatty acid molecules on the nanoparticles. At $0.25 < R < 0.50$, the SANS profile shows a behavior intermediate between discrete patches and continuous layer, which is critical in programming the interfacial binding of the fatty acid-nanoparticle complex (discussed in section 2.5). In summary, the SANS shows that the morphology of the fatty acid adsorbed on the $m\mathrm{SiO_2}$ nanoparticles changes from discrete patches to the continuous layer upon increasing R. While the origin of such morphological transitions of the fatty acid self-assemblies is not clear from SANS data, molecular dynamic simulations can provide detailed insight into the assembly process (discussed below).

2.4. Molecular Dynamic Simulations. The addition of the counterion (ethanolamine) drives a morphological change in the self-assembled state of fatty acid onto $m\mathrm{SiO_2}$ nanoparticles. We use molecular dynamics (MD) simulations to understand the mechanism of self-assembly of fatty acid molecules on the surface of $m\mathrm{SiO_2}$. All simulations were performed using GROMACS 4.6.3[41] and visualized in VMD.[42] In our simulations, the amount of fatty acid was kept constant, and the counterion molar ratio was systematically increased from R = 0.1 to 1.0. More details about the simulation setup are shown in Table S1. In a typical simulation run, a mixture of unionized (protonated) fatty acid and deprotonated fatty acid with protonated counterion molecules corresponding to different R values was randomly placed above the $m\mathrm{SiO_2}$ surface. The mixture together with the $m\mathrm{SiO_2}$ surface was solvated in a water box using the TIP3P model.[43] Energy minimization followed by 500-ps NVT pre-equilibration using

https://dx.doi.org/10.1021/acs.langmuir.0c00156
Langmuir 2020, 36, 3703−3712

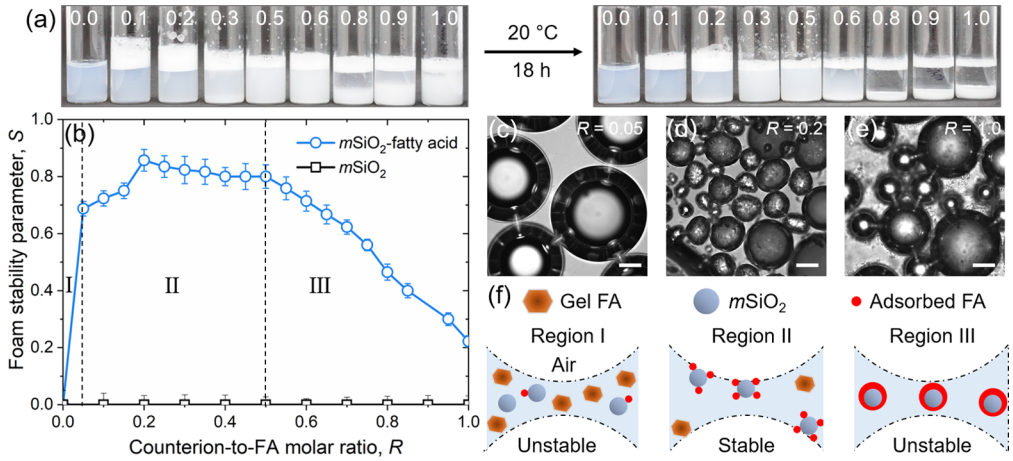

Figure 5. (a) Photographs of the change in foam volume for the fatty acid−mSiO$_2$ mixture with increasing counterion-to-fatty acid molar ratio, R. (b) The change in foam stability of mSiO$_2$ and fatty acid aqueous solution quantified using foam stability parameter, S as a function of R. Three distinct regions of foam stability with increasing R can be identified, namely, (I) rapid increase, (II) constant, and (III) slow decrease (blue circles and line). The foam stability parameter for mSiO$_2$ aqueous solution in the absence of fatty acid remains 0 (black squares) for all tested R values. (c)−(e) Micrographs of bubbles formed at R = 0.05, R = 0.2, and R = 1.0, respectively, at fixed mSiO$_2$ and fatty acid concentration. The images show that the bubbles become nonspherical with the increasing amount of counterion and then recover to the spherical shape as more counterions is added. The scale bars correspond to 20 μm. (f) Schematics representing the mechanism of change in foam stability of the fatty acid−mSiO$_2$ mixtures with increasing R.

a V-rescale thermostat[44] was performed to stabilize the temperature of the simulation box to 298 K. Next, to stabilize the pressure to 1 bar, 500-ps NPT simulations were carried out using the leapfrog algorithm[45] with a time step of 0.1 fs, and the Parrinello−Rahman thermostat[46] is applied until the simulation box was equilibrated at 1 bar. Finally, the simulations were performed in NPT ensemble for 20 ns for data collection. A particle−particle particle−mesh algorithm with an analytical derivative (P3M-AD)[47] is used for long-range electrostatic interactions.

Snapshots extracted from the last step of the equilibration trajectory at various R values are shown in Figure 4a−f. We find that the fatty acid molecules assemble as a large patch at R < 0.2 and form a continuous layer at R = 1.0. In the range of 0.2 < R < 1.0, several discrete assemblies are formed on mSiO$_2$. Apart from the shape, the mean size of surface assemblies referenced to the bare silica surface, D_h is plotted as a function of R in Figure 4g. At low counterion addition (at R = 0.1), a single large assembly is bound to mSiO$_2$ via negatively charged carboxylate ions highlighted as red spheres (Figure 4a). As R is increased to 0.5 (Figure 4d), the bulky assembly decomposes into two small patches with one of them being a bilayer. The decomposition and spreading process of fatty acid assemblies at R = 0.5 leads to decrease of D_h as shown in Figure 4g. As R is further increased above 0.5 (R = 0.7 and 1.0), a continuous layer of fatty acid structure can be observed as shown in Figure 4e,f. The decrease of D_h upon increasing R from 0.1 to 1.0 (i.e., a decrease in the size of the self-assembled surface aggregates of fatty acid on mSiO$_2$) is in agreement with the shift of the primary form factor oscillation in the SANS profile to higher wave vector as shown in Figure 3b.

The assembled state of fatty acid molecules is governed by (a) electrostatic attraction between the deprotonated fatty acid molecules (carboxylate ions) and the mSiO$_2$ surface, and (b) the van der Waals attraction between the hydrocarbon tails of the neighboring fatty acid molecules on the particle surface. To understand the driving force that triggers the morphological change, the electrostatic interaction[47] (E_{elec}) between fatty acid and mSiO$_2$ and the van der Waals interaction (E_{vdW}) among fatty acid alkyl chains at different R values are calculated and shown in Figure 4h,i, respectively. At R < 0.2, a small fraction of fatty acid molecules exist in the deprotonated state and adsorb onto mSiO$_2$ by an electrostatic attraction. In our simulations, we find that at R = 0.1, the fatty acid assembly is composed of 4 deprotonated fatty acid molecules and 66 fatty acid molecules, and the weakly negative-charged portions of the surface aggregate serve as adsorption sites, immobilizing the bulky assembly at the positive-charged sites. At R > 0.2, an increasing number of deprotonated fatty acid molecules are bound to mSiO$_2$ via an electrostatic attraction (red spheres in Figure 4a). At R = 0.5, the number of deprotonated fatty acid molecules is equal to that of protonated fatty acid molecules. The electrostatic interaction between fatty acid and mSiO$_2$ and the van der Waals attraction between the hydrocarbon chains of the molecules are both significant. Therefore, small fatty acid assemblies comprising both protonated and deprotonated fatty acid molecules are adsorbed onto the mSiO$_2$ surface where the deprotonated fatty acid molecules act as electrostatic linkers to mSiO$_2$. For R > 0.7, the majority of fatty acid molecules are present in their carboxylate forms. The mSiO$_2$-bound deprotonated fatty acid molecules first form a packed monolayer by the lateral organization of the alkyl chains via van der Waals attraction, and the excess deprotonated fatty acid molecules are then packed to the monolayer to form a thin bilayer. Thus, the increased E_{elec} between fatty acid assemblies and mSiO$_2$ together with decreased E_{vdW} between fatty acid molecules drives the morphological transition of fatty acid assembly from a large patch to a thin bilayer upon increasing R. These observations on the morphological transition of fatty acid molecules on mSiO$_2$ nanoparticles with increasing R agree with the SANS experiments (see section 2.3).

2.5. Foam Stability in Fatty Acid−mSiO$_2$ Aqueous Solution. The foam stability of fatty acid soaps in aqueous solution is known to be related to the morphology of fatty acid assemblies at the air−water interface. However, the origin of

https://dx.doi.org/10.1021/acs.langmuir.0c00156
Langmuir 2020, 36, 3703−3712

superior foam observed in mixtures of oppositely charged nanoparticles and amphiphiles is not well understood. Here, we aim to interrelate the state of fatty acid assemblies formed on mSiO$_2$ nanoparticles with their ability to stabilize the air−water interface (i.e., foam). The stability of foams formed by the mixture of fatty acid and mSiO$_2$ with increasing R was tested at pH 6. A typical foaming experiment was performed using an aqueous mixture of 0.02 M fatty acid and 1.0 wt % mSiO$_2$ with increasing R from 0.0 to 1.0. The used concentration of fatty acid was equivalent to Γ_{max} at R = 1.0. The foam was produced from the fatty acid and mSiO$_2$ mixture by vigorous shaking, and it was kept undisturbed at room temperature for 18 h. The change in the foam volume of the mixture after 18 h is monitored using digital imaging as shown in Figure 5a. The stability of the foam produced by the fatty acid−mSiO$_2$ mixture at a given R is quantified using a foam stability parameter, S, represented as $S = v_{final}/v_{initial}$ where $v_{initial}$ and v_{final} are the volumes of foam immediately after shaking and after 18 h of equilibration, respectively. For R = 0, the foam stability parameter was equal to zero since no foam could be produced from the pure fatty acid and mSiO$_2$ mixture without a counterion (Figure 5a,b). By adding a small amount of counterions (R = 0.05), S increased from 0 to 0.7. By further increasing R, S reached a plateau value around 0.8 from R = 0.2 to 0.5. For R > 0.5, S decreased to a final value of 0.2 at R = 1 (Figure 5b). From these results, we define three regions of foam stability. Region I corresponds to low foam stability for 0 < R < 0.05. Region II, 0.05 < R < 0.5, corresponds to high foam stability. Region III also corresponds to a low foam stability regime for 0.5 < R < 1.0. We further investigate the origin of change in foam stability with increasing R by microscale imaging of the bubbles in all three identified regions for R = 0.05, 0.2, and 1.0 (Figure 5c−e). In region I, the bubbles were spherical, highlighting the large interfacial tension between air and water. Transforming from region I to region II, the shape of bubbles undergoes a change from smooth sphere to rippled nonspherical. This change in the shape of the bubble upon increasing R can be attributed to the adsorption of the fatty acid−mSiO$_2$ complex at the air−water interface and corresponding interfacial jamming of the nanoparticles. We believe that the adsorption of fatty acid patches onto mSiO$_2$ makes the nanoparticles partially hydrophobic, driving its adsorption onto the air−water interface. Following such interfacial adsorption, the shape transformation of the bubbles is driven by two key factors: (a) jamming of nanoparticles in the thin films between the bubbles upon liquid drainage hindering the relaxation of the bubbles to spherical shape;[48,49] and (b) compression of liquid films by nanoparticle jamming causing the buckled and rough appearance of the bubble surface.[50,51] Furthermore, we observe that the shape of bubbles recovers to a smooth sphere from rippled perturbed sphere upon increasing R to 1.0 (region III). It should be noted that no foam could be formed by mixture of mSiO$_2$ and the counterion, highlighting the critical role of fatty acid in the foaming process (Figure 5b, squares).

In region I, only a few patches of fatty acid molecules are present at the mSiO$_2$ surfaces (sections 2.3 and 2.4), which induce enough amphiphilicity to adsorb at the air−water interface. Therefore, hydrophilicity and weak amphiphilic characters of the nanoparticles in region I resulted in the lack of foam stability. In region II, the number of fatty acid patches at the particle surface was enough to reach an appropriate contact angle value, which leads to the adsorption of particles at the air−water interface. The patchy particles formed a dense layer at the interface protecting the bubbles against coalescence and coarsening due to jamming phenomenon, thus leading to the observed stable foams. In the region III, the fatty acid formed a continuous bilayer structure on the mSiO$_2$ nanoparticle surface, leading to hydrophilic surface and diminishing the interfacial activity of the fatty acid-nanoparticle complex. This lack of interfacial activity of fatty acid−nanoparticle complex destabilizes the air bubbles and leads to poor foam stability (sections 2.3 and 2.4). Thus, the fatty acid−mSiO$_2$ nanoparticles stay in the liquid phase and sediment to the bottom of solution due to the fatty acid-mediated heteroaggregation of the mSiO$_2$ nanoparticles (Figure 5a,e). This absence of nanoparticles at the air−water interface spontaneously drives the bubble coalescence, drainage, and coarsening without any physical or energetic barrier(s). These foaming experiments highlight a direct relationship between the fatty acid structure on mSiO$_2$ and their interfacial property. We find that patches of fatty acid on mSiO$_2$ nanoparticles are necessary for increasing the interfacial activity of the complex and enhancing the corresponding foam stability. We show that the self-assembled state of fatty acid molecules on mSiO$_2$ directs the interfacial activity of the composite nanostructure and the resulting macroscopic properties such as foam stability. The strong correlation between the self-assembled state of fatty acid molecules on the surface of mSiO$_2$ nanoparticles and foam stability leads to the formation of programmable foams for which the stability can be tuned by modifying R.

3. CONCLUSIONS

This study presents the effect of the counterion-to-fatty acid molar ratio, R, on the self-assembled state of fatty acid molecules on aminopropyl-modified silica nanoparticles. We show that the maximum amount of fatty acid that can be adsorbed on the mSiO$_2$ increases with increasing R. The increase in the amount of fatty acid molecules adsorbed on positively charged mSiO$_2$ nanoparticles (at pH 6) is driven by an increase in the number of negatively charged deprotonated fatty acid molecules upon increasing R. The increase in the maximum surface excess of fatty acid on mSiO$_2$ with increasing R drives a morphological change in the self-assembled state of fatty acids at the nanoparticle surface from discrete patches to the continuous layer. The control over that morphological state of fatty acid on mSiO$_2$ by changing R enables programming the hydrophilic/hydrophobic characteristics of the fatty acid−mSiO$_2$ nanoparticle complex. At low R, the fatty acid molecules form large discrete patches on the surface of mSiO$_2$, which decompose and spread on mSiO$_2$ to form a continuous layer at high R, evidenced by the analysis of SANS profiles and MD simulations. This morphological change is induced by the increased electrostatic interaction between fatty acid and mSiO$_2$ along with the decreased van der Waals interaction between fatty acid molecules upon increasing R. The self-assembled state of fatty acid on the surface of mSiO$_2$ is strongly correlated with the interfacial activity of the complex. We demonstrate that the foam stability of the mixture can be directed by altering the adsorbed state of the fatty acid molecules onto mSiO$_2$ by changing the counterion-to-fatty acid molar ratio. This study provides a fundamental basis to comprehend the nontrivial effects of counterions on morphological evolution and phase transition of fatty acid assemblies formed on nanoparticles. Further work on such modified silica nanoparticle and their dispersion with fatty acid

https://dx.doi.org/10.1021/acs.langmuir.0c00156
Langmuir 2020, 36, 3703−3712

can facilitate new principles of designing ultrastable foams valuable in cosmetics and food industries.[52,53]

■ ASSOCIATED CONTENT

Supporting Information

The Supporting Information is available free of charge at https://pubs.acs.org/doi/10.1021/acs.langmuir.0c00156.

Characterization of silica nanoparticles using SAXS and zeta potential-pH titration, amount of undissolved fatty acid at different R values, surface tension calibration curve, surface tension of fatty acid at $R = 0$, surface area-to-volume ratio determined by Porod's analysis of SANS profile, derivation of raspberry model under core contrast matched condition, and MD simulation setup (PDF)

■ AUTHOR INFORMATION

Corresponding Author

Bhuvnesh Bharti − *Cain Department of Chemical Engineering, Louisiana State University, Baton Rouge, Louisiana 70803, United States;* orcid.org/0000-0001-9426-9606; Email: bbharti@lsu.edu

Authors

Yingzhen Ma − *Cain Department of Chemical Engineering, Louisiana State University, Baton Rouge, Louisiana 70803, United States*

Yao Wu − *Cain Department of Chemical Engineering, Louisiana State University, Baton Rouge, Louisiana 70803, United States*

Jin Gyun Lee − *Cain Department of Chemical Engineering, Louisiana State University, Baton Rouge, Louisiana 70803, United States*

Lilin He − *Neutron Scattering Division, Oak Ridge National Laboratory, Oak Ridge, Tennessee 37831, United States*

Gernot Rother − *Chemical Sciences Division, Oak Ridge National Laboratory, Oak Ridge, Tennessee 37831, United States;* orcid.org/0000-0003-4921-6294

Anne-Laure Fameau − *National Institute of French Agriculture Research, Nantes 44300, France;* orcid.org/0000-0002-8237-2216

William A. Shelton − *Cain Department of Chemical Engineering and Center for Computation and Technology, Louisiana State University, Baton Rouge, Louisiana 70803, United States;* orcid.org/0000-0003-4280-5109

Complete contact information is available at: https://pubs.acs.org/10.1021/acs.langmuir.0c00156

Notes

The authors declare no competing financial interest.

■ ACKNOWLEDGMENTS

The article is dedicated to the memory of Prof. Gerhard H. Findenegg (TU Berlin), who was a great scholar, scientist, and mentor. Authors thank Mr. Y. Guo for assistance with SEM imaging and Prof. Kerry Dooley for helping with nitrogen gas adsorption measurement. The research was supported by U.S. Department of Energy, Office of Science, Basic Energy Sciences, under EPSCoR grant no. DE-SC0012432 with additional support from the Louisiana Board of Regents. This research used resources at the High Flux Isotope Reactor, DOE Office of Science User Facilities operated by the Oak Ridge National Laboratory. Portions of this research were conducted with high-performance computing resources provided by Louisiana State University. Contributions to measurements and manuscript preparation by G. R. were supported by the U.S. Department of Energy, Office of Science, Office of Basic Energy Sciences, Chemical Sciences, Geosciences and Biosciences Division.

■ REFERENCES

(1) Pileni, M. P. Nanosized Particles Made in Colloidal Assemblies. *Langmuir* **1997**, *13*, 3266−3276.

(2) Bharti, B.; Fameau, A. L.; Rubinstein, M.; Velev, O. D. Nanocapillarity-Mediated Magnetic Assembly of Nanoparticles into Ultraflexible Filaments and Reconfigurable Networks. *Nat. Mater.* **2015**, *14*, 1104−1109.

(3) Foster, L. M.; Worthen, A. J.; Foster, E. L.; Dong, J.; Roach, C. M.; Metaxas, A. E.; Hardy, C. D.; Larsen, E. S.; Bollinger, J. A.; Truskett, T. M.; et al. High Interfacial Activity of Polymers "Grafted through" Functionalized Iron Oxide Nanoparticle Clusters. *Langmuir* **2014**, *30*, 10188−10196.

(4) Li, C.; Yu, X.; Somasundaran, P. Effect of a Comb-like Amphiphilic Polymer on the Stability of Alumina Dispersions. *Colloids Surf.* **1992**, *69*, 155−158.

(5) Lee, J.; Lee, S. J.; Choi, J. Y.; Yoo, J. Y.; Ahn, C. H. Amphiphilic Amino Acid Copolymers as Stabilizers for the Preparation of Nanocrystal Dispersion. *Eur. J. Pharm. Sci.* **2005**, *24*, 441−449.

(6) Smith, A. M.; Duan, H.; Rhyner, M. N.; Ruan, G.; Nie, S. A Systematic Examination of Surface Coatings on the Optical and Chemical Properties of Semiconductor Quantum Dots. *Phys. Chem. Chem. Phys.* **2006**, *8*, 3895−3903.

(7) Binks, B. P.; Murakami, R. Phase Inversion of Particle-Stabilized Materials from Foams to Dry Water. *Nat. Mater.* **2006**, *5*, 865−869.

(8) Maestro, A.; Rio, E.; Drenckhan, W.; Langevin, D.; Salonen, A. Foams Stabilised by Mixtures of Nanoparticles and Oppositely Charged Surfactants: Relationship between Bubble Shrinkage and Foam Coarsening. *Soft Matter* **2014**, *10*, 6975−6983.

(9) Ahmed, S.; Wunder, S. L. Effect of High Surface Curvature on the Main Phase Transition of Supported Phospholipid Bilayers on SiO 2 Nanoparticles. *Langmuir* **2009**, *25*, 3682−3691.

(10) Bharti, B.; Meissner, J.; Gasser, U.; Findenegg, G. H. Surfactant Adsorption and Aggregate Structure at Silica Nanoparticles: Effects of Particle Size and Surface Modification. *Soft Matter* **2012**, *8*, 6573−6581.

(11) Lugo, D. M.; Oberdisse, J.; Lapp, A.; Findenegg, G. H. Effect of Nanoparticle Size on the Morphology of Adsorbed Surfactant Layers. *J. Phys. Chem. B* **2010**, *114*, 4183−4191.

(12) Meissner, J.; Wu, Y.; Jestin, J.; Shelton, W. A.; Findenegg, G. H.; Bharti, B. PH-Induced Reorientation of Cytochrome c on Silica Nanoparticles. *Soft Matter* **2019**, *15*, 350−354.

(13) Fameau, A. L.; Zemb, T. Self-Assembly of Fatty Acids in the Presence of Amines and Cationic Components. *Adv. Colloid Interface Sci.* **2014**, *207*, 43−64.

(14) Arnould, A.; Cousin, F.; Chabas, L.; Fameau, A. L. Impact of the Molar Ratio and the Nature of the Counter-Ion on the Self-Assembly of Myristic Acid. *J. Colloid Interface Sci.* **2018**, *510*, 133−141.

(15) Cross, L. C.; Klyne, W. Iupac Commission on Nomenclature of Organic Chemistry. *Rules Nomencl. Org. Chem.* **1976**, *67*, 13−30.

(16) Fameau, A. L.; Cousin, F.; Saint-Jalmes, A. Morphological Transition in Fatty Acid Self-Assemblies: A Process Driven by the Interplay between the Chain-Melting and Surface-Melting Process of the Hydrogen Bonds. *Langmuir* **2017**, *33*, 12943−12951.

(17) Marangoni, A. G.; Acevedo, N.; Maleky, F.; Co, E.; Peyronel, F.; Mazzanti, G.; Quinn, B.; Pink, D. Structure and Functionality of Edible Fats. *Soft Matter* **2012**, *8*, 1275−1300.

(18) Fameau, A.-L.; Houinsou-Houssou, B.; Ventureira, J. L.; Navailles, L.; Nallet, F.; Novales, B.; Douliez, J.-P. Self-Assembly, Foaming, and Emulsifying Properties of Sodium Alkyl Carboxylate/

Guanidine Hydrochloride Aqueous Mixtures. *Langmuir* **2011**, *27*, 4505−4513.
(19) Crowe, J. H.; McKersie, B. D.; Crowe, L. M. Effects of Free Fatty Acids and Transition Temperature on the Stability of Dry Liposomes. *Biochim. Biophys. Acta, Biomembr.* **1989**, *979*, 7−10.
(20) Florindo, C.; Romero, L.; Rintoul, I.; Branco, L. C.; Marrucho, I. M. From Phase Change Materials to Green Solvents: Hydrophobic Low Viscous Fatty Acid-Based Deep Eutectic Solvents. *ACS Sustainable Chem. Eng.* **2018**, *6*, 3888−3895.
(21) Zana, R. Partial Phase Behavior and Micellar Properties of Tetrabutylammonium Salts of Fatty Acids: Unusual Solubility in Water and Formation of Unexpectedly Small Micelles. *Langmuir* **2004**, *20*, 5666−5668.
(22) Fameau, A.; Saint-Jalmes, A.; Cousin, F.; Houinsou Houssou, B.; Novales, B.; Navailles, L.; Nallet, F.; Gaillard, C.; Boué, F.; Douliez, J. Smart Foams: Switching Reversibly between Ultrastable and Unstable Foams. *Angew. Chem., Int. Ed.* **2011**, *50*, 8264−8269.
(23) Meissner, J.; Prause, A.; Bharti, B.; Findenegg, G. H. Characterization of Protein Adsorption onto Silica Nanoparticles: Influence of PH and Ionic Strength. *Colloid Polym. Sci.* **2015**, *293*, 3381−3391.
(24) Kneuer, C.; Sameti, M.; Haltner, E. G.; Schiestel, T.; Schirra, H.; Schmidt, H.; Lehr, C. M. Silica Nanoparticles Modified with Aminosilanes as Carriers for Plasmid DNA. *Int. J. Pharm.* **2000**, *196*, 257−261.
(25) Bharti, B.; Meissner, J.; Findenegg, G. H. Aggregation of Silica Nanoparticles Directed by Adsorption of Lysozyme. *Langmuir* **2011**, *27*, 9823−9833.
(26) Wu, Y.; Ma, Y.; He, L.; Rother, G.; Shelton, W. A.; Bharti, B. Directed Pore Uptake and Phase Separation of Surfactant Solutions under Confinement. *J. Phys. Chem. C* **2019**, *123*, 9957−9966.
(27) Wang, X.; Sun, T.; Teja, A. S. Density, Viscosity, and Thermal Conductivity of Eight Carboxylic Acids from (290.3 to 473.4) K. *J. Chem. Eng. Data* **2016**, *61*, 2651−2658.
(28) MacLeod, C. A.; Radke, C. J. A Growing Drop Technique for Measuring Dynamic Interfacial Tension. *J. Colloid Interface Sci.* **1993**, 435−448.
(29) Lee, J. G.; Larive, L. L.; Valsaraj, K. T.; Bharti, B. Binding of Lignin Nanoparticles at Oil−Water Interfaces: An Ecofriendly Alternative to Oil Spill Recovery. *ACS Appl. Mater. Interfaces* **2018**, *10*, 43282−43289.
(30) Langmuir, I. The Constitution and Fundamental Properties of Solids and Liquids. *J. Am. Chem. Soc.* **1917**, *39*, 1848−1906.
(31) Zhou, X.; Zhou, X. The Unit Problem in the Thermodynamic Calculation of Adsorption Using the Langmuir Equation. *Chem. Eng. Commun.* **2014**, *201*, 1459−1467.
(32) Liu, Y. Is the Free Energy Change of Adsorption Correctly Calculated? *J. Chem. Eng. Data* **2009**, *54*, 1981−1985.
(33) Biswas, S. C.; Chattoraj, D. K. Kinetics of Adsorption of Cationic Surfactants at Charcoal-Water Interface. *J. Surf. Sci. Technol.* **1998**, *14*, 78−92.
(34) Bharti, B.; Xue, M.; Meissner, J.; Cristiglio, V.; Findenegg, G. H. Assembling Wormlike Micelles in Tubular Nanopores by Tuning Surfactant-Wall Interactions. *J. Am. Chem. Soc.* **2012**, *134*, 14756−14759.
(35) Müter, D.; Shin, T.; Demé, B.; Fratzl, P.; Paris, O.; Findenegg, G. H. Surfactant Self-Assembly in Cylindrical Silica Nanopores. *J. Phys. Chem. Lett.* **2010**, *1*, 1442−1446.
(36) Zemb, T.; Lindner, P. *Neutron, X-Rays and Light. Scattering Methods Applied to Soft Condensed Matter*; 1*st Edition*, Elsevier, 2002.
(37) Nampoothiri, P. K.; Gandhi, M. N.; Kulkarni, A. R. Effect of Surface Grafting Coefficient and Chain Length of Fatty Acids on the Luminescence of Neodymium3+−Doped LaF3nanoparticles. *J. Mater. Chem. C* **2015**, *3*, 1817−1822.
(38) Larson-Smith, K.; Jackson, A.; Pozzo, D. C. Small Angle Scattering Model for Pickering Emulsions and Raspberry Particles. *J. Colloid Interface Sci.* **2010**, *343*, 36−41.
(39) Despert, G.; Oberdisse, J. Formation of Micelle-Decorated Colloidal Silica by Adsorption of Nonionic Surfactant. *Langmuir* **2003**, *19*, 7604−7610.
(40) Pedersen, J. S.; Gerstenberg, M. C. Scattering Form Factor of Block Copolymer Micelles. *Macromolecules* **1996**, *29*, 1363−1365.
(41) Hess, B.; Kutzner, C.; Van Der Spoel, D.; Lindahl, E. GRGMACS 4: Algorithms for Highly Efficient, Load-Balanced, and Scalable Molecular Simulation. *J. Chem. Theory Comput.* **2008**, *4*, 435−447.
(42) Humphrey, W.; Dalke, A.; Schulten, K. VMD: Visual Molecular Dynamics. *J. Mol. Graphics* **1996**, *14*, 33−38.
(43) Bjelkmar, P.; Larsson, P.; Cuendet, M. A.; Hess, B.; Lindahl, E. Implementation of the CHARMM Force Field in GROMACS: Analysis of Protein Stability Effects from Correction Maps, Virtual Interaction Sites, and Water Models. *J. Chem. Theory Comput.* **2010**, *6*, 459−466.
(44) Bussi, G.; Donadio, D.; Parrinello, M. Canonical Sampling through Velocity Rescaling. *J. Chem. Phys.* **2007**, *126*, No. 014101.
(45) Hockney, R. W.; Goel, S. P.; Eastwood, J. W. Quiet High-Resolution Computer Models of a Plasma. *J. Comput. Phys.* **1974**, *14*, 148−158.
(46) Nosé, S. A Molecular Dynamics Method for Simulations in the Canonical Ensemble. *Mol. Phys.* **1984**, *52*, 255−268.
(47) Buneman, O. *Computer Simulation Using Particles*; Hockney, R. W.; Eastwood, J. W., CRC Press, 1983, *25* (3), 422−425.
(48) Subramaniam, A. B.; Abkarian, M.; Mahadevan, L.; Stone, H. A. Colloid Science: Non-Spherical Bubbles. *Nature* **2005**, *438*, 930.
(49) Binks, B. P.; Kirkland, M.; Rodrigues, J. A. Origin of Stabilisation of Aqueous Foams in Nanoparticle-Surfactant Mixtures. *Soft Matter* **2008**, *4*, 2373−2382.
(50) Binks, B. P.; Horozov, T. S. Aqueous Foams Stabilized Solely by Silica Nanoparticles. *Angew. Chem., Int. Ed.* **2005**, *44*, 3722−3725.
(51) Martinez, A. C.; Rio, E.; Delon, G.; Saint-Jalmes, A.; Langevin, D.; Binks, B. P. On the Origin of the Remarkable Stability of Aqueous Foams Stabilised by Nanoparticles: Link with Microscopic Surface Properties. *Soft Matter* **2008**, *4*, 1531.
(52) Denkov, N. D.; Tcholakova, S.; Golemanov, K.; Ananthpadmanabhan, K. P.; Lips, A. The Role of Surfactant Type and Bubble Surface Mobility in Foam Rheology. *Soft Matter* **2009**, *5*, 3389−3408.
(53) Xi, Y.; Wolf, C. M.; Pozzo, L. D. Self-Assembly of Donor−Acceptor Conjugated Polymers Induced by Miscible 'Poor' Solvents. *Soft Matter* **2019**, *15*, 1799−1812.

https://dx.doi.org/10.1021/acs.langmuir.0c00156
Langmuir 2020, 36, 3703−3712